Effects of composition and pore evolution on thermophysical properties of Huadian oil shale in retorting and oxidizing pyrolysis

Effects of composition and pore evolution on thermophysical properties of Huadian oil shale in retorting and oxidizing pyrolysis

Shaotao Xu [a,b,c], Youhong Sun [a,b,c,d,*], Xiaoshu Lü [a,e,f], Qinchuan Yang [a,b,c], Qiang Li [a,b,c], Zhendong Wang [g], Mingyi Guo [a,b,c,*]

[a] College of Construction Engineering, Jilin University, Changchun 130021, China
[b] National-Local Joint Engineering Laboratory of In-situ Conversion, Drilling and Exploitation Technology for Oil Shale, Jilin University, Changchun 130021, China
[c] Key Lab of Ministry of Natural Resources for Drilling and Exploitation Technology in Complex Conditions, Jilin University, Changchun 130021, China
[d] China University of Geosciences, Beijing 100083, China
[e] Department of Civil and Structural Engineering, School of Engineering, Aalto University, PO Box 12100, FIN-02015 Espoo, Finland
[f] Department of Electrical Engineering and Energy Technology, University of Vaasa, P.O.Box 700, FIN-65101, Vaasa, Finland
[g] Key Laboratory of Coal Exploration and Comprehensive Utilization, Ministry of Nature and Resources, Shaanxi Coal Geology Group Co., Ltd., Xi'an 710021, China

Keywords:
Oil shale
Oxidizing pyrolysis
Pore evolution
Chemical composition
Thermophysical property

A B S T R A C T

This chemical composition and pore evolution of oil shale during oxidizing pyrolysis (OP) and their influences on its thermophysical properties were investigated in this study. Various transformations of the minerals in oil shale were detected, among which montmorillonite was noted to transform into illite during anaerobic retorting (AR), and into kaolinite during OP. Variations in the quantities of residual carbon and organic matter during low-temperature AR and OP were noted to be possibly responsible for the difference in pore volumes. Remarkable increases in surface and volumes of mesopores and macropores through OP were observed even at low temperatures. The pore volume was proven to significantly affect the thermophysical properties of semi-cokes at low temperatures during OP. Higher thermal conductivity and thermal diffusivity were observed in semi-cokes obtained via OP at 350 °C compared to those obtained via AR at 520 °C. These phenomena highlight the potential of OP for application in in-situ oil shale exploitation.

1. Introduction

The increase in energy demand and low levels of oil resources have necessitated urgent research on alternative energy [1,2]. Oil shale, a fine-grained sedimentary rock containing organic matter (kerogen) that can be converted into shale oil and gas, has attracted considerable attention as an auxiliary energy source owing to its abundant reserves and wide distribution [3–6]. Compared to directly burning oil shale as a power-plant fuel to generate electricity, aboveground retorting and in-situ pyrolysis of kerogen to yield oil and gas is currently more prevalent [6,7]. Among these extraction methods, in-situ retorting is the most promising technology for extracting liquid or gaseous hydrocarbons from wells by directly heating underground oil shale formations to avoid adverse environmental effects [4,6–7].

Recent efforts have focused on demonstrating in-situ pyrolysis technologies to develop an optimal strategy regarding heat input for the oil shale formation. The utilization of the heat of exothermic reaction between residual carbon (produced during pyrolysis) and injected oxygen to facilitate underground kerogen pyrolysis has attracted attention [7–9,36]. For instance, a self-heating retorting strategy was developed to spontaneously increase the retorting temperature in the absence of external heat supply by taking advantage of the reactions of residual carbon and oxygen [7,10–11]. Co-current oxidizing pyrolysis is known to enhance the chemical reactivity of organic matter in oil shale and reduce the initial decomposition temperature of organic matter [8]. A low energy-consumption strategy denoted as the topochemical reaction method was demonstrated by our group, in which heat is generated for self-pyrolysis of kerogen by partially oxidizing kerogen in the presence of small quantities of air [9,12]. These studies point to the importance of introducing oxygen in kerogen pyrolysis to significantly reduce the energy input; this is likely to be the most promising strategy for in-situ conversion and utilization of oil shale.

Another key issue regarding the in-situ exploitation of oil shale involves the use of the heat input to rapidly heat the oil shale formation to

* Corresponding authors at: College of Construction Engineering, Jilin University, Changchun 130021, China.
E-mail addresses: syh@jlu.edu.cn (Y. Sun), guomingyi@jlu.edu.cn (M. Guo).

Table 1
Proximate, ultimate and Fischer assay analysis results of the raw oil shale (performed three times).

Proximate analysis (wt.%, ad)		Sd	Ultimate analysis (wt.%, d)		Sd
Moisture	1.12	0.22	C	31.59	0.07
Volatile matter	43.24	0.26	H	3.99	0.03
Ash	54.26	0.14	N	0.30	0.02
Fixed carbon	1.38	0.21	S	0.79	0.01
Calorific value (MJ/kg)	12.02	0.08	O	9.06	0.02
Fischer assay analysis (wt.%, ad)					
Shale oil	18.31	0.18			
Water	3.79	0.09			
Semi-coke	67.39	0.18			
Gases	10.51	0.15			

Note: ad: air dried. d: dried. Sd: Standard deviation.

the pyrolysis temperature [13]. Therefore, the thermophysical properties of oil shale, such as thermal conductivity (λ), thermal diffusivity (K), and volumetric specific heat capacity (C_v), are decisive factors for realizing in-situ production of shale oil, and directly affect the heat transfer process and thermal cracking of kerogen.

The thermal properties of most rocks are known to be dependent on the bulk density, porosity, grain (crystal) size and shape, cementation, formation pressure, temperature, anisotropy, mineral composition, and the nature of saturating fluids [13–20]. The thermal conductivity of consolidated rocks is known to be predominantly controlled by the composition of rock solids and saturating fluid, and porosity [18]. Generally, an increase in temperature increases the porosity and decreases the thermal conductivity of shale [16], whereas larger grain sizes lead to a decrease in thermal contact resistance and an increase in the thermal conductivity [17]. The specific heat of rocks can be predicted using the sum of the specific heats of the constituents weighted according to their mass fractions [18]. Similarly, an increase in temperature leads to a decrease in thermal diffusivity, which is positively correlated with rock crystallinity and inversely proportional to porosity [19,20].

Although several studies have investigated the thermophysical properties of rocks, those of oil shale during oxidizing pyrolysis (OP) have not been thoroughly examined. Therefore, the composition and pore evolution of oil shale during OP at different temperatures and their influence on its thermophysical properties were systematically investigated in this study. The superiority of thermophysical properties resulting from the OP process for in-situ oil shale exploitation was confirmed, which highlights the potential of in-situ OP for oil shale production.

2. Materials and methods

2.1. Materials

The raw oil shale used in this study was obtained from Huadian, Jilin province, China. The results of proximate, ultimate and Fischer assay analyses of raw oil shale used in this study are shown in Table 1. The raw oil shale was crushed and screened to 0.4–1.7-mm-sized particles, and subsequently dried in the oven at 80 °C for 10 h before initiating the experiment.

2.2. Experiment

The experimental apparatus used in this study is shown in Fig. 1. The OP procedure was conducted as follows: First, 20 g of raw oil shale was placed on a wire mesh in a quartz retort (internal diameter, 50 mm; height, 140 mm). The wire mesh was employed to ensure complete contact between oil shale and oxygen during pyrolysis. The oil shale samples were subsequently heated from ambient temperature (20 °C) to temperatures of 350, 400, and 520 °C at a heating rate of 10 °C/min by external heating in N_2. When the target temperature was reached, N_2 was switched to pure O_2 at ambient temperature. External heat was subsequently employed to maintain samples at the target temperature without any further heating for 2 h. During the experiment, the external temperature of the sample was monitored and maintained using a thermocouple, whereas the internal temperature of the sample varied because of kerogen pyrolysis, the self-heating effect, and other reactions. Semi-cokes were collected after the experiment when the setup naturally cooled down. Semi-cokes pyrolyzed in N_2 (anaerobic retorting; AR) under similar temperature conditions were also prepared for comparison. During all experiments, the flow rates of nitrogen and oxygen were maintained at 80 mL/min using a flow control device. Owing to the low oxygen-flow-rate, oil shale could be stably oxidized and pyrolyzed without the light and flame phenomena of the combustion reaction even at 520 °C; a high oil yield could be obtained, which has been previously demonstrated by our group [10].

The OP and AR processes at different temperatures are denoted as **O_2-350**, **O_2-400**, **O_2-520**, **N_2-350**, **N_2-400**, and **N_2-520**, respectively; the first part of the notation indicates the pyrolysis atmosphere and the second part refers to the target temperature. The semi-cokes obtained from the various pyrolysis processes are correspondingly denoted as **SO350**, **SO400**, **SO520**, **SN350**, **SN400**, and **SN520**, respectively. Moreover, the raw oil shale is denoted as **Sraw**.

2.3. Analytical methods

Thermogravimetric (TG) analysis was performed using an STA 449 F3 thermal analyser (Netzsch, Germany). The flow rates of protective gas (nitrogen) and the carrier gas (air) are 20 mL/min and 60 mL/min, respectively. 10 mg (±0.5 mg) sample was used in all the tests to reduce the influence of temperature gradients and heat and mass transfer effects. The samples were heated from 30 to 900 °C at a rate of 10 °C/min. Duplicate experiments were performed to ensure reproducibility and the error of mass loss and temperature was less than ± 0.5 wt% and ± 1 °C, respectively. Fourier transform infrared (FTIR) spectra were recorded on a Nicolet iS10 FTIR spectrometer (Thermo Nicolet, U. S. A). The samples were finely grinded to the wright 4 mg and homogenized with 100 mg of ground KBr (dried under an infrared lamp) and the spectra were

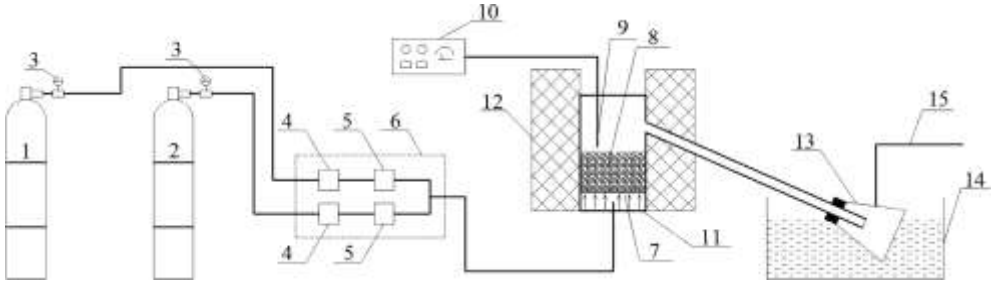

Fig. 1. Schematic diagram of the experimental apparatus (1: N_2 steel cylinder; 2: O_2 steel cylinder; 3: pressure gauge; 4: mass flowmeter; 5: flow controller; 6: flow control system; 7: wire mesh; 8: specimen; 9: thermocouple; 10: temperature control panel; 11: quartz retort; 12: furnace; 13: conical flask; 14: condenser; 15: vent).

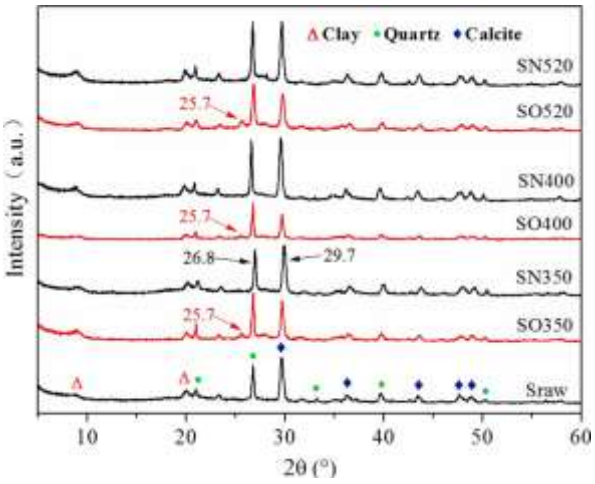

Fig. 2.X-ray diffractogram of raw oil shale and various semi-cokes.

collected in the mid-IR region from 4000 to 400 cm^{-1}. Low-temperature nitrogen adsorption−desorption analysis was performed using a Kubo-X1000 specific surface meter (Builder, China). 1000 mg of the sample was used in each experiment, and sample was cooled by 196 °C liquid nitrogen during the experiment. X-ray diffraction (XRD) patterns were measured using a D2 PHASER diffractometer (Bruker, Germany) and Cu Kα radiation at a step length of 0.02°/s. Ultimate analysis was performed using a vario MICRO cube elemental analyzer (Elementer, Germany). The pressure of high purity oxygen is 0.20 MPa and the temperature of combustion furnace is 960 °C. Thermophysical properties were investigated using a TPS 2500S thermal constants analyser (Hot disk, Sweden). Prior to the experiments, the raw oil shale or semi-coke was ground into fine powder, and the fraction passing through a 200-mesh sieve (63 μm) was used further. Subsequently, 5 g of the powder was compressed into 6-mm-thick cylindrical blocks under pressures of 67, 100, and 134 MPa, respectively, for 10 min for the analysis of thermophysical properties. The surface morphologies of the powder samples were analysed using field-emission scanning electron microscopy (FESEM; S-4800, Hitachi, Japan), with an acceleration voltage of 3. 0 kV.

Before conducting the analytical experiments, the prepared samples were finely ground and subsequently passed through a 63-μm sieve. The raw oil shale or semi-coke powder (0.1 g) was dissolved in 20 mL of deionized water to measure the pH value.

3. Results and discussion

3.1. Composition of minerals in semi-cokes

3.1.1. XRD analysis

Oil shale is known to be primarily composed of organic matter and an inorganic mineral skeleton, typically consisting of quartz (silicates), clay, different types of carbonates ($CaCO_3$, $MgCO_3$, and dolomite), and pyrite. [21,22]. The XRD patterns (Fig. 2) show that clay, quartz, and calcite are the primary minerals in used oil shale. As shown in Fig. 2, semi-cokes obtained via OP show different X-ray characteristic peaks from raw oil shale and semi-cokes obtained via AR. For instance, the intense peak at 29.7°, which corresponds to calcite, exhibits a marked decrease compared to the strong peak representing quartz at 26.8° in semi-cokes obtained via OP. And a new peak appears at 25.7° in **SO350**, **SO400**, and **SO520**, whereas the decline in peak intensity and appearance of the 25.7° peak do not occur in **SN350**, **SN400**, and **SN520**. Because quartz only undergoes phase transformation during the heating and cooling processes and its content remains unchanged, a portion of the calcite is decomposed or decrystallized, and new minerals (identified as kaolinite in the mineral composition analysis) are generated during OP.

3.1.2. Mineral composition analysis

The contents of the mineral components of semi-cokes were measured to determine the changes revealed by the XRD patterns. Fig. 3 clearly indicates that new mineral components, such as kaolinite and

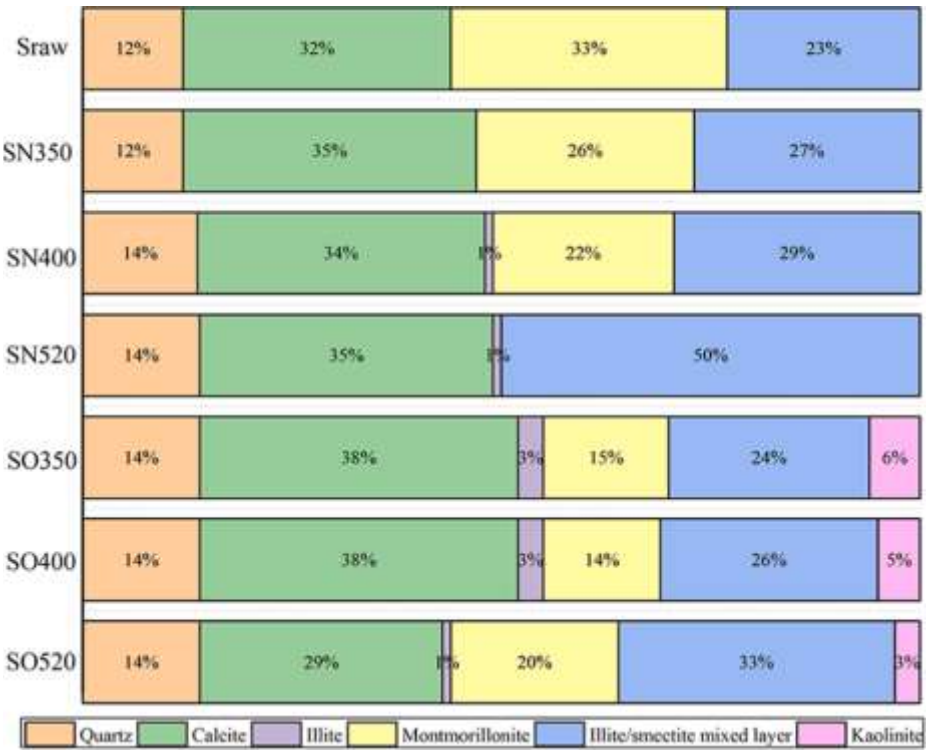

Fig. 3. Contents of mineral components of raw oil shale and various semi-cokes.

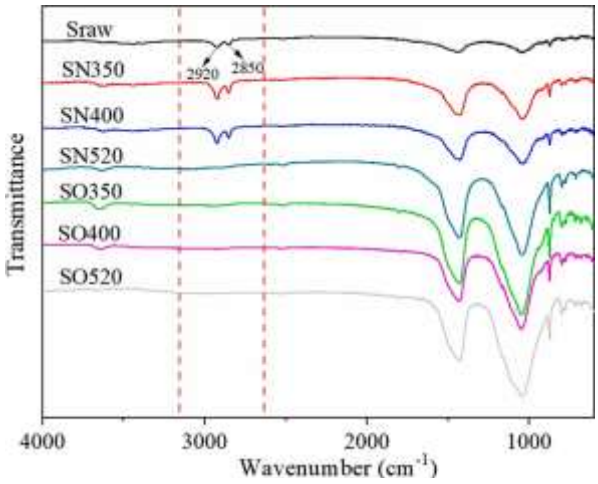

Fig. 4.FTIR spectra of oil shale and various semi-cokes.

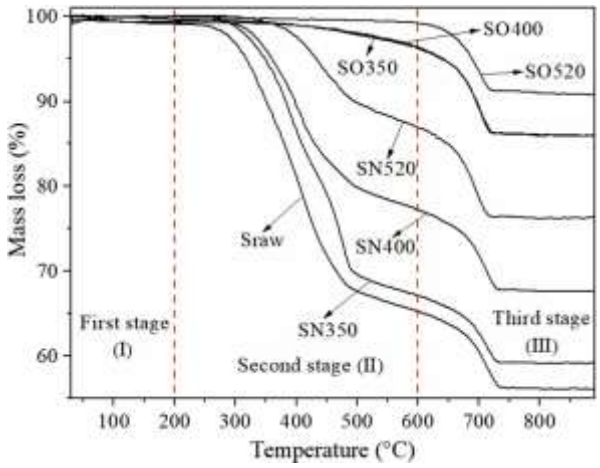

Fig. 5.TG analysis of oil shale and the various semi-cokes.

illite, are produced in the semi-cokes. Previous studies have revealed that montmorillonite can be transformed into illite in alkaline envi- ronments and kaolinite in acidic environments via heat treatment [23,24]. During AR, the content of montmorillonite in semi-cokes de- creases, whereas the content of the illite/montmorillonite mixed layer increases with increasing temperatures; illite is noted to be present in **SN400** and **SN520**. The pH values indicate that all investigated semi- coke aqueous solutions and water products are alkaline; therefore, a part of montmorillonite in the oil shale possibly transforms into illite at high temperatures in an alkaline environment during AR, and the degree of transformation is directly proportional to the temperature.

On the other hand, montmorillonite is noted to simultaneously transform into kaolinite and illite during OP, and the amounts of illite and kaolinite decrease with the increasing temperatures. The pH values indicate that the semi-cokes and water products obtained via OP are alkaline; therefore, acidic products (nitrogen oxides, sulphur oxides, or organic acids) are presumed to be produced via OP of oil shale at high temperatures, which causes the transformation of montmorillonite to kaolinite. However, the presence of acidic products was not detected, which is possibly owing to the neutralisation of acidic products during migration in an alkaline environment.

Fig. 3 shows that the content of calcite in **SO520** is lower than that in **SO350** and **SO400**, whereas the ratio of calcite to quartz in **SO350** and **SO400** are higher than that in **Sraw** and **SN400**. Because the XRD patterns (Fig. 2) indicate that a small amount of calcite was decomposed or decrystallized during OP, some of the calcite in **SO520** is presumed to decompose, whereas the calcite in **SO350** and **SO400** undergoes phase transformation and becomes amorphous. Because the decomposition temperature of calcite is above 700 °C [9,25], the organic matter or residual carbon in oil shale reacts exothermically with oxygen, which ensures that the internal temperature of oil shale exceeds the external temperature and temporarily reaches 700 °C; this facilitates decomposition of a part of the calcite component during the **O_2-520** process. This phenomenon of increasing temperature is consistent with that reported in previous studies [7,11]. The miniscule increases in calcite and quartz contents of **SO350** and **SO400** are possibly owing to the decrease in the content of clay minerals caused by decomposition.

3.2. Organic residues and residual carbon in semi-cokes

3.2.1. FTIR analysis

The FTIR spectra of oil shale and the various semi-cokes are shown in Fig. 4. The bands at 2920 and 2850 cm^{-1} are attributed to the characteristic peaks of C–H bonds of saturated aliphatic hydrocarbons, corresponding to the kerogen in oil shale [12,26,27]. These two bands are

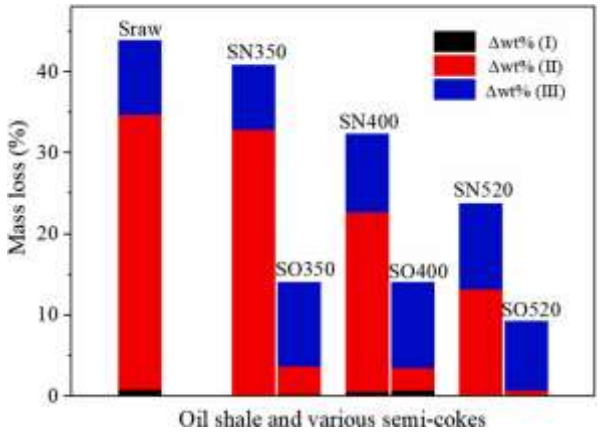

Fig. 6. Weight losses of oil shale and semi-cokes at different stages.

present in the **SN350** and **SN400** spectra but vanish in the **SN520** spectrum. This indicates that the alkyl groups still exist at temperatures above 400 °C; however, they completely decompose below 520 °C during AR. These two peaks completely disappear in the **SO350** spectrum, which suggests that the alkyl groups are entirely decomposed below 350 °C during OP [10].

3.2.2. TG analysis

Fig. 5 shows the results of TG analysis of the oil shale and various semi-cokes. Generally, kerogen in oil shale is converted into substantial amounts of residual carbon, oil, and gas after heat treatment during AR, which results in a large amount of residual carbon in the semi-cokes [8,26]. As shown in Fig. 5, all the TG curves can be divided into three stages [12,27–30]. The first stage (I) (below 200 °C) is primarily attributed to the evaporation of water, including that of some interlayer water from minerals [30]. The second stage (II) (200–600 °C) is dominated by the oxidation of kerogen, organic residues, and residual carbon [29,30]. The third stage (III) (greater than 600 °C) is ascribed to the decomposition of calcite [27,28].

The weight losses of oil shale and semi-cokes at different stages of the experiments are presented in Table S1 and Fig. 6. The weight loss in the second stage in **Sraw** is 33.86%, which corresponds to the content of kerogen [30,31]. The second-stage weight losses in **SN350**, **SN400**, and **SN520** are 32.84%, 22.23% and 13.14%, respectively, and indicate a gradually decreasing trend. This is attributed to the increasing amount of pyrolyzed kerogen with increasing temperatures. Only ~ 1.02% of the kerogen is cracked in the **N_2-350** process, and more than 11.63% of

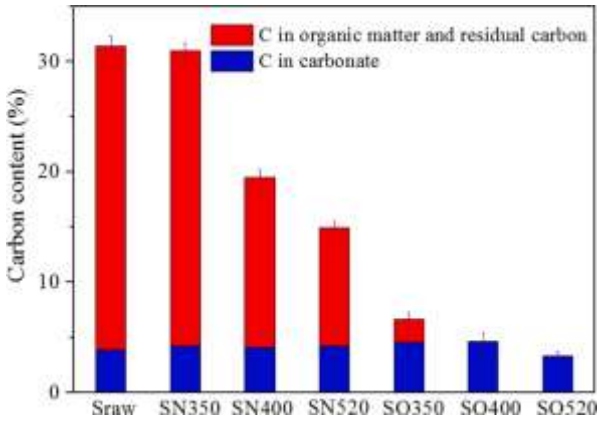

Fig. 7. Carbon content of oil shale and the different semi-cokes.

kerogen is pyrolyzed in the **N_2-400** process. The FTIR results of the **N_2-520** process indicate that almost all the kerogen is pyrolyzed in **SN520,** which implies that ~ 13.14% of the residual carbon remains.

The second-stage weight loss in semi-cokes obtained via OP follows a similar trend, with samples exhibiting values of 3.44% (**SO350**), 2.73% (**SO400**), and 0.71% (**SO520**). This suggests that only ~ 3.44% of organic residues remain in **SO350**, and kerogen has almost completely been oxidized in **SO520**. Moreover, this indicates that only a small amount of organic residues exists in the semi-coke obtained through OP even at low pyrolysis temperatures. This is consistent with observations made by Guo et al. [10].

3.2.3. Carbon content analysis

Carbon (C) in oil shale is known to originate from organic matter and carbonates [26,27]. Table S2 and Fig. 7 show the results of C content analysis in the various semi-cokes. The TG and FTIR results were noted to indicate the complete oxidation of kerogen in **SO520**, which implies that all of the C (nearly 3.33%) originates from carbonate. Therefore, the carbonate ($CaCO_3$) content in **SO520** is estimated to be 27.75% (3.33% $\times$100/12), which is similar to that obtained via mineral composition analysis (29%). Conversely, the C content in carbonates can be calculated and the C in organic matter and residual carbon can be obtained via subtraction and using the results of mineral composition analysis. These results show that the semi-cokes obtained via AR contain large amounts of C in the form of organic matter and residual carbon, which decreases with increasing temperatures. However, with respect to OP, **SO350** contains only a small amount of C from organic matter and residual carbon owing to the effect of oxygen, and almost none of the C is present in **SO400** and **SO520**.

3.3. Pore evolution of semi-cokes

3.3.1. Nitrogen adsorption–desorption analysis

The nitrogen adsorption–desorption method is extensively used to examine the pore shape and structure of fossil fuels [27]. Fig. 8 shows the nitrogen adsorption–desorption isotherms of the oil shale and various semi-cokes. Type IV isotherms are obtained, according to the IUPAC classification, which indicates the presence of numerous meso- pores in the oil shale and semi-cokes [22,32,33]. Additionally, all the hysteresis loops of the different curves in Fig. 8 are similar to the H3 hysteresis loop based on IUPAC classification, which indicates that all investigated samples contain slit-like pores [22].

The pore structure parameters of oil shale and the various semi-cokes are presented in Table S3 and Fig. 9. The results indicate the presence of only 2–50-nm-sized mesopores and macropores (greater than 50 nm) in the semi-cokes [27]. During AR, the amount of mesopores decreases from that in **Sraw** to that in **SN350**, and subsequently increases from that in **SN350** to that in **SN520** (0.0164 to 0.0442 cm^3/g) with increasing temperatures; the amount of macropores increases from that in **Sraw** to that in **SN520**. These results indicate that the slight pyrolysis of kerogen, softening and coking of organic matter, and evaporation of interlayer water in clay minerals result in the disappearance of original pores and inhibit the formation of new pores in the **N_2-350** process. More kerogen is subsequently converted into oil and gas with increasing temperatures, leading to the substantial production of mesopores and macropores. This result is consistent with that reported by Bai et al. [27] and Liu et al. [32].

Unlike in the AR process, the amounts of both mesopores and macropores considerably increase during OP even at low temperatures. The mesopore volume almost reaches the maximum from 0.0397 cm^3/g (**Sraw**) to 0.5125 cm^3/g (**SO350**); a slight subsequent increase from that in **SO350** to that in **SO400**, and a decrease from that in **SO400** to **SO520** can be observed. The macropore volume consistently increases from 0.0164 cm^3/g (**Sraw**) to 1.6879 cm^3/g (**SO520**). This is attributed to the large decomposition of kerogen in an oxidizing atmosphere even at low temperatures [10], which produces numerous mesopores and macropores. The decomposition of calcite in the **O_2-520** process leads to pore collapse and interconnection (visible in the SEM images), which results in a slight decrease and significant increase in the number of mesopores and macropores, respectively.

Fig. 10 shows the total specific surface area (SSA) and pore volume (PV) of the oil shale and different semi-cokes. The SSA and PV are evaluated using the Brunauer–Emmett–Teller (BET) model and the Barrett–Joyner–Halenda (BJH) theory according to the desorption branch, respectively [32]. The results show that SSA and PV exhibit similar trends in the AR process. At the beginning, slight declines in SSA from 2.7413 to 1.2785 m^2/g and in PV from 0.0163 to 0.0159 cm^3/g are noted between the **Sraw** and **SN350** samples. Subsequently, a sustained increasing trend is observed, including a considerable increase from the properties of **SN400** to those of **SN520**; finally, an SSA of 29.2036 m^2/g and a PV of 0.1005 cm^3/g are achieved. The reason behind this change involves the same explanation presented for mesopores in the semi-cokes of AR processes; this result is consistent with those reported by Bai et al. [27].

However, SSA and PV exhibit different trends during OP. At the beginning, a considerable increase in the SSA of **Sraw** to that of **SO350** (2.7413 to 24.8694 m^2/g) occurs. The SSA subsequently reaches a maximum at 34.4628 m^2/g in **SO400**, and slightly decreases to 31.3156 m^2/g in **SO520**. PV exhibits a continuously increasing trend from 0.0163 cm^3/g (**Sraw**) to 0.1658 cm^3/g (**SO520**). The change in SSA can be explained in a manner similar to that presented for mesopores, and that in PV follows a logic similar to that discussed for macropores in the semi-cokes obtained via OP [27].

3.3.2. SEM analysis

Fig. 11 shows the SEM images of the raw oil shale and various semi-cokes. As shown in Fig. 11, a small amount of mesopores are visible in **SN350** during AR, and softening phenomena occur on certain areas of the surface. Obvious cracks and fractures can be seen in **SN400**, along with certain macropores, which are attributed to the violent release of oil and gas. In the **SN520** sample, the pores are almost completely open, the surface lamellar structure is developed, and the number of irregular macropores significantly increases. This is consistent with the results reported by Bai et al. [27].

With respect to OP, numerous fractures are visible in **SO350**, and a large number of mesopores and macropores appear owing to the transformation of large amounts of kerogen into oil and gas and precipitation at low temperatures [7,10]. The further development of this phenomenon in **SO400** indicates that the transformation of kerogen further intensifies. In **SO520**, numerous adjacent pores collapse and merge, and the degree of irregularity of the surface structure further increases, which is related to the decomposition of carbonate. The SEM results are consistent with those obtained from nitrogen adsorption analysis.

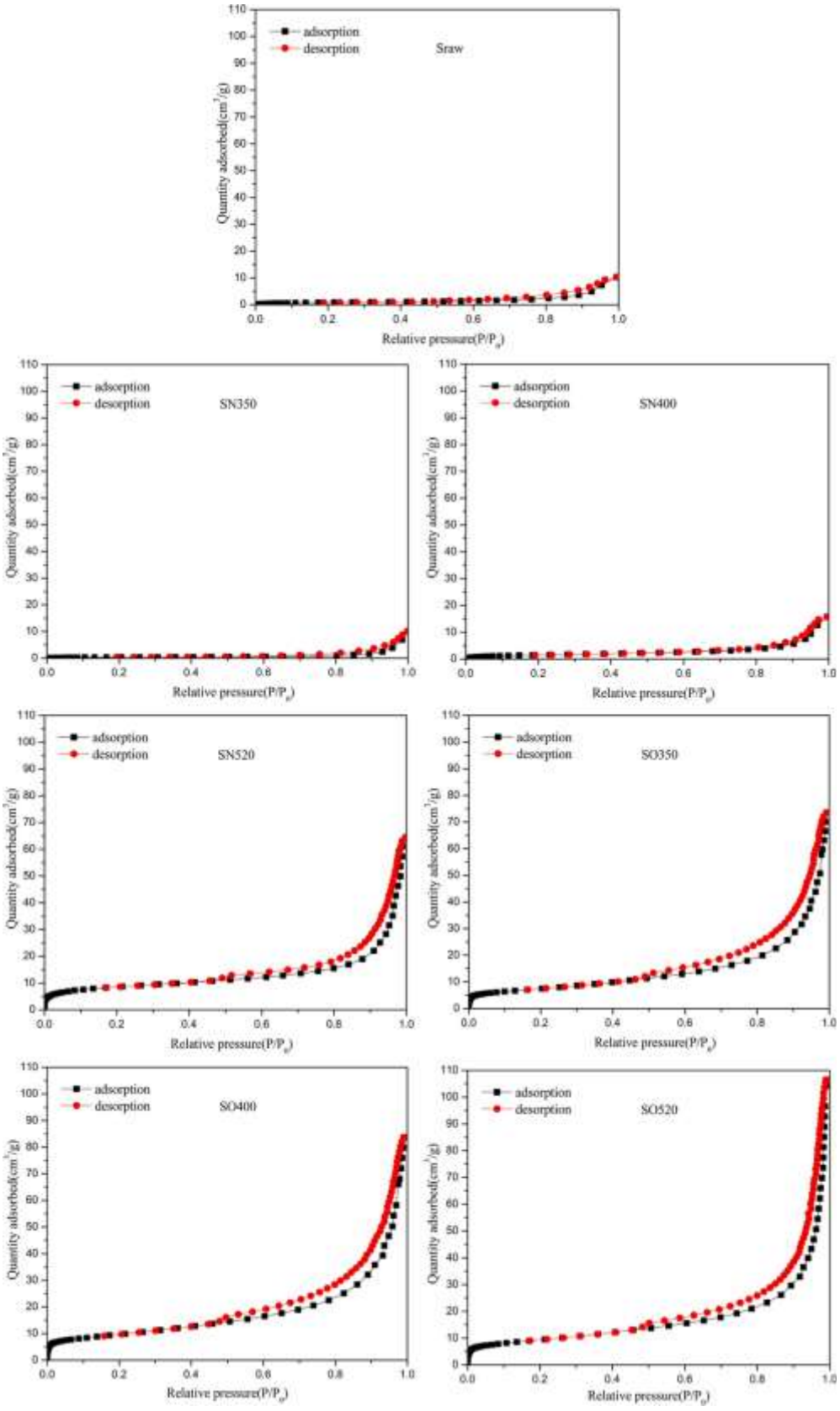

Fig. 8. Adsorption–desorption isotherms of oil shale and the various semi-cokes.

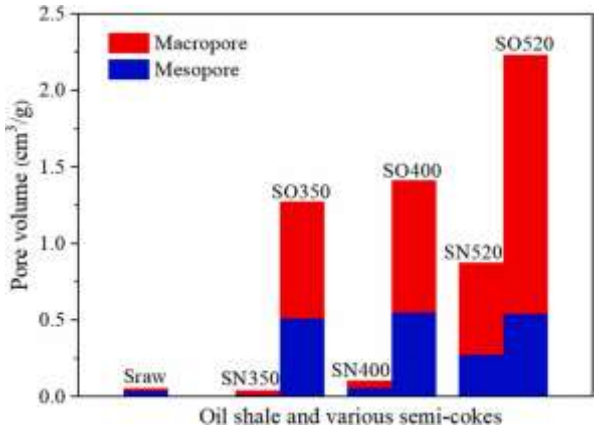

Fig. 9. Amount of mesopores and macropores in oil shale and semi-cokes via nitrogen adsorption.

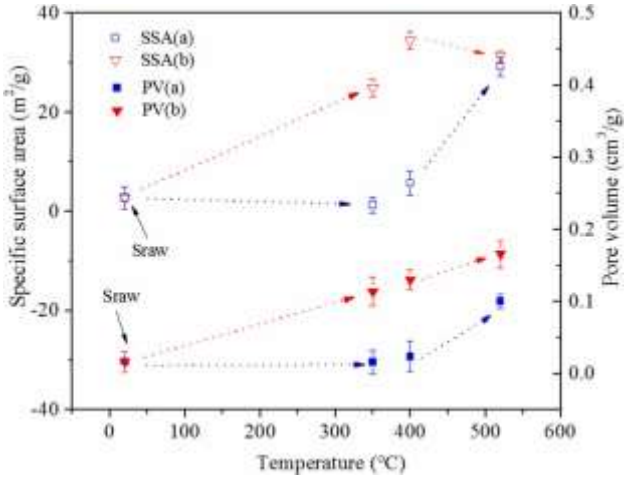

Fig. 10. Total BET specific surface area (SSA) and pore volume (PV) of oil shale and semi-cokes obtained via (a) AR and (b) OP processes.

3.4. Thermophysical properties of semi-cokes

Various heat and mass transfer processes occur in oil shale with different particle sizes upon heating. For instance, small oil shale particles exhibit rapid heating rates and low product-transfer resistance, leading to thorough pyrolysis in a short duration, which impedes the secondary reaction of pyrolysis products [34]. However, regardless of the size of semi-cokes, they have almost identical chemical compositions and pore structures after sufficient pyrolysis at identical temperatures, because particle sizes have a negligible effect on the final degree of pyrolysis of Huadian oil shale [34,35]. Therefore, the study of thermophysical properties and the influence of small oil shale and semi-coke particles is crucial for the in-situ exploitation of oil shale.

The thermophysical properties of oil shale and semi-cokes, such as thermal conductivity (λ), thermal diffusivity (K), and volumetric specific heat capacity (C_v), are listed in Table S4; these were measured by pressing the synthesized powder into cylindrical blocks to reduce the inhomogeneity of samples. These three parameters are related by the following equation [13,14]:

$$\lambda = K \cdot C_V$$

To ensure that the chemical composition and pore volume are the only two significant factors that affect the thermophysical properties, sample preparation methods such as particle size control, drying, and block pressing under identical pressures were employed to eliminate the influence of grain (crystal) size and shape, cementation, formation pressure, anisotropy, saturating fluids, and other factors on the thermophysical properties [16]. Table S5 shows the thermophysical properties of certain materials in relation to the components of oil shale and semi-cokes. Table S5 indicates that larger pore volumes, which imply the presence of drier air, result in a lower conductivity and specific heat capacity, whereas higher amounts of residual carbon leads to a higher conductivity [16,18]. Additionally, the pyrolysis of kerogen leads to a decrease in the content of organic matter, which increases the specific gravity of other components such as quartz and carbonate in oil shale, resulting in higher thermal conductivity [16].

3.4.1. Thermal conductivity

The thermal conductivity results in Fig. 12 indicate that from **Sraw** to **SN350**, thermal conductivity slightly changes owing to small changes in organic matter content and pore volume. The thermal conductivity of samples under different pressures all exhibit a trend that first increases and then decreases from **SN350** to **SN520**. These results indicate that the pyrolysis of kerogen and generation of residual carbon are the primary factors that increase the thermal conductivity, whereas the decrease is primarily caused by the considerable increase in pore volume owing to the pyrolysis of kerogen [16,18].

The thermal conductivity of samples obtained via the OP process exhibits a trend similar to that of the AR process. The PV and SSA significantly increase while the organic matter content considerably decreases from those in **Sraw** to **SO350**. The results indicate that the thermal conductivity changes slightly, which implies that the effects of organic matter content and pore volume variation in the semi-coke offset each other. Subsequently, the amount of cracked or oxidized kerogen and pore volume both slightly increase from those in **SO350** to those in **SO400**, and thermal conductivity slightly increases as well, indicating the significant effect of the decrease in organic matter content. Finally, PV and SSA considerably increase with respect to the **SO400** to **SO520** samples owing to the decomposition of partial calcite. The results indicate that thermal conductivity dramatically decreases, which suggests that the large increase in pore volume is the primary factor behind this decrease [16]. The semi-coke blocks obtained via AR and OP processes under different pressures all exhibit a similar variation in thermal conductivity, which proves the reliability of the aforementioned analysis.

3.4.2. Volumetric specific heat capacity

Fig. 13 shows the variations in volumetric specific heat capacity of samples obtained via OP and AR processes. From the results of thermophysical properties of pressed samples, the thermophysical properties of pressed samples are closer to the natural block samples with the increase of pressing pressure. The results reveal that the variation in volumetric specific heat capacity of the block pressed at 67 MPa is slightly different from that of the other two blocks, which is possibly caused by the influence of intergranular pores formed during pressing owing to the lower pressing pressure.

Except for the semi-coke block pressed at 67 MPa, the other two semi-coke blocks exhibit similar variation in volume specific heat capacity. The volumetric specific heat capacity slightly decreases from that in **Sraw** to that in **SN350** in AR owing to the precipitation of interlayer water in clay [18,30]. Subsequently, from **SN350** to **SN400**, a portion of kerogen is pyrolyzed and a large amount of residual carbon is generated; however, the pore volume slightly increases, resulting in a slight increase in volumetric specific heat capacity. Finally, a significant decline from **SN400** to **SN520** is noted, which is primarily caused by the large increase in pore volume owing to the complete pyrolysis of kerogen [18,27].

However, the results show that the volumetric specific heat capacity significantly decreases from that in **Sraw** to that in **SO350** in the OP processes, primarily owing to the large amount of pore volume formed by the decomposition of kerogen at low temperatures. Subsequently, the

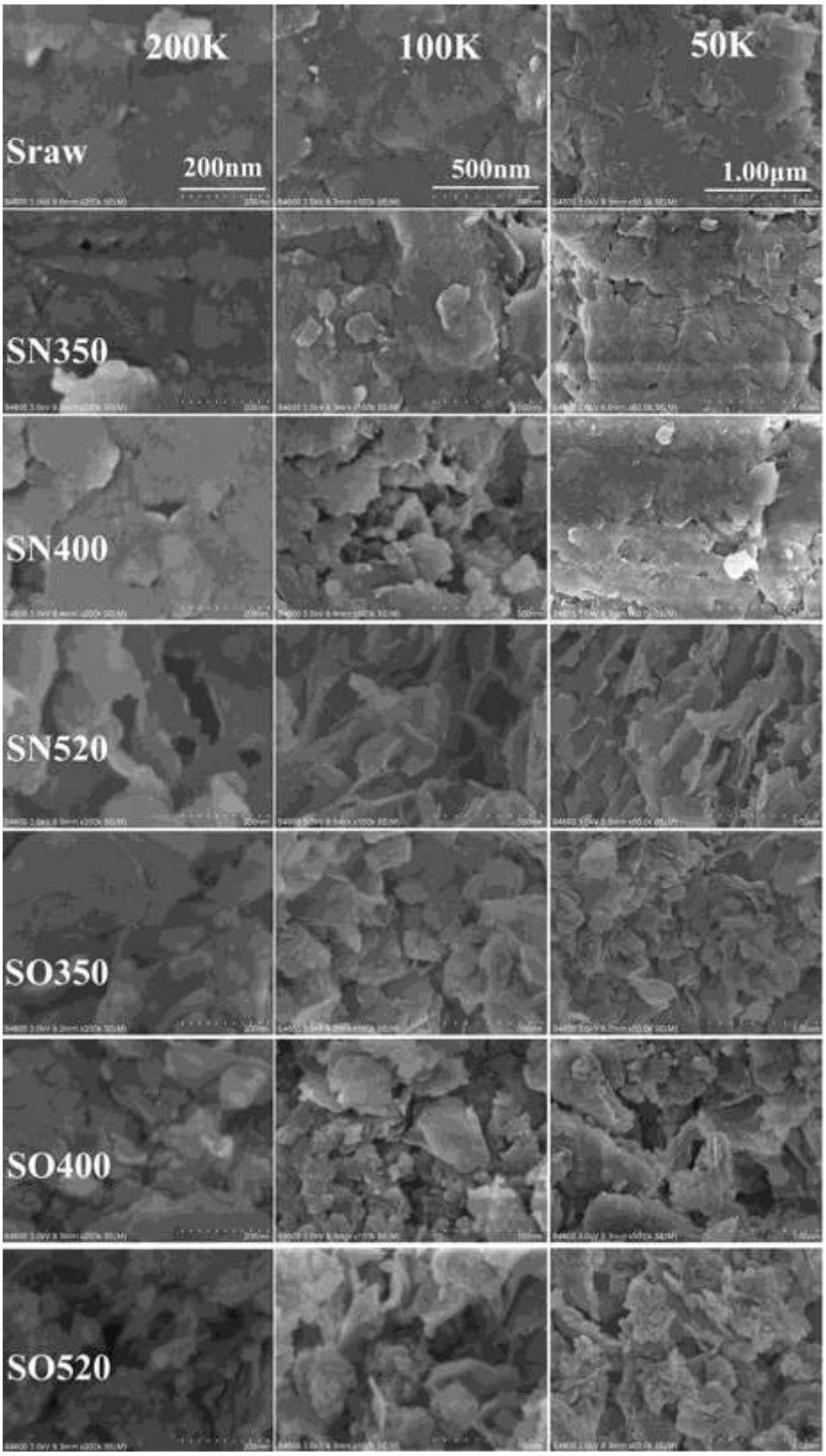

Fig. 11.SEM images of the raw oil shale and various semi-cokes.

pore volume increases from that in **SO350** to that in **SO400**, and the organic matter content slightly decreases. These results suggest that the volumetric specific heat capacity exhibits a slight increase, indicating that the decrease in organic matter content has a greater impact. Finally, the pore volume of **SO400** considerably increases to that in **SO520** owing to the decomposition of partial calcite, leading a decrease in volumetric specific heat capacity [18].

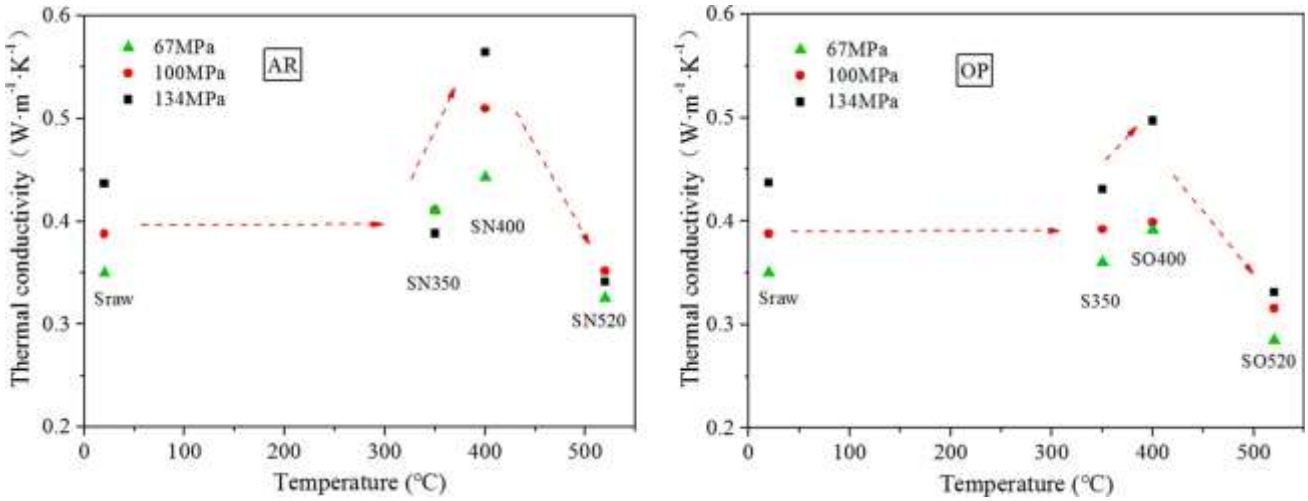

Fig. 12. Thermal conductivity (λ) of different cylindrical blocks containing oil shale and that of different semi-cokes via AR and OP processes.

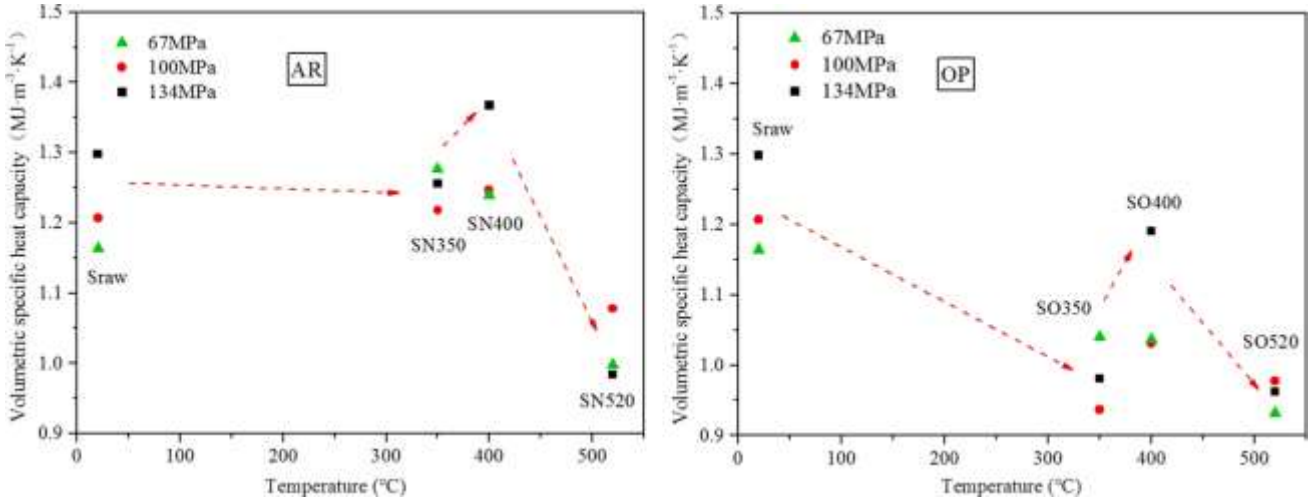

Fig. 13. Volumetric specific heat capacity (C_v) of different cylindrical blocks containing oil shale and that of different semi-cokes via AR and OP processes.

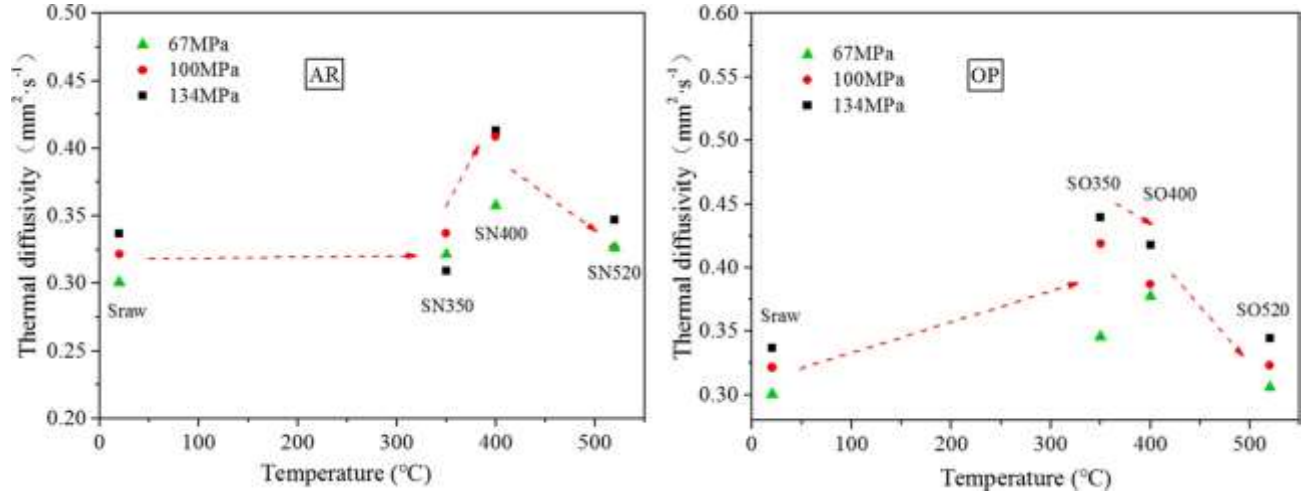

Fig. 14. Thermal diffusivity (K) of different cylindrical blocks containing oil shale and that of different semi-cokes via AR and OP processes.

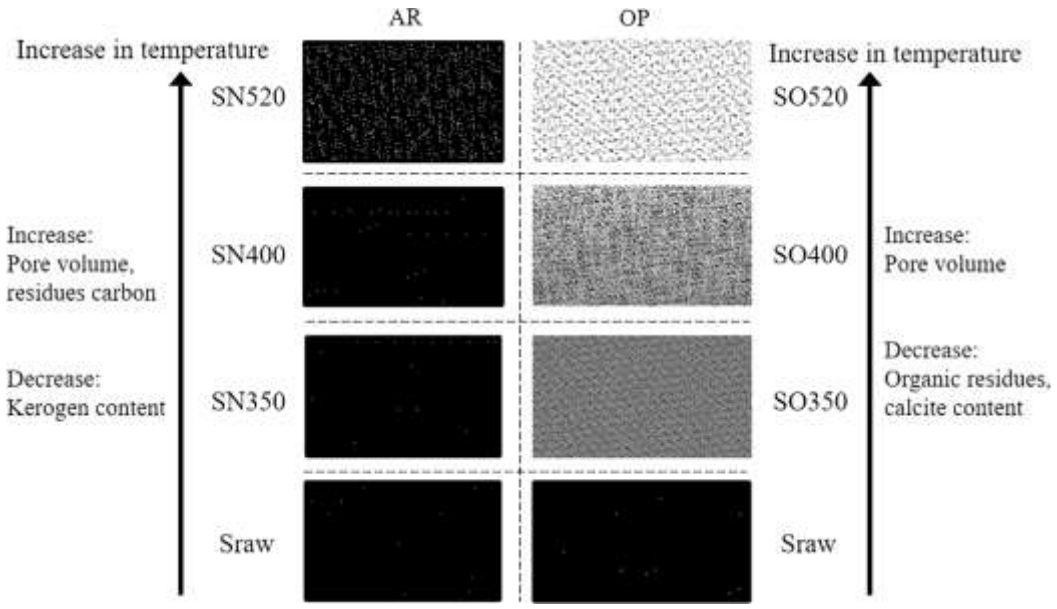

Fig. 15. Plausible mechanism of the influence of composition and pore evolution on thermophysical properties of semi-cokes.

3.4.3. Thermal diffusivity

The measured thermal diffusivity values are shown in Fig. 14. Because thermal diffusivity can be obtained by dividing the thermal conductivity by volumetric specific heat capacity at a constant pressure [13,14], Fig. 14 data can be also be obtained by dividing the values in Fig. 12 by the corresponding values in Fig. 13.

The results indicate only a few changes in thermal diffusivity from that of **Sraw** to that of **SN350**, and a trend that first increases and then decreases is subsequently noted with respect to **SN350** and **SN520**. Because the thermal conductivity and volumetric specific heat capacity exhibit similar variations in the AR process, the ratios of changes in thermal conductivity and volumetric specific heat capacity from those of **Sraw** to those of **SN350** are almost identical. Subsequently, the increase in the ratio of thermal conductivity is greater than that of volumetric specific heat capacity with respect to **SN350** and **SN400**, and the decrease in the ratio of thermal conductivity is greater than that of volumetric specific heat capacity with respect to **SN400** and **SN520**.

In the OP process, the results indicate that the thermal diffusivity significantly increases from that in **Sraw** to that in **SO350**, and subsequently exhibits a continuously decreasing trend from **SO350** to **SO520**, except for the semi-coke block pressed at 67 MPa. The thermal conductivity slightly changes from that in **Sraw** to that in **SO350**, whereas the volumetric specific heat capacity decreases, resulting in a decrease in the thermal diffusivity. The thermal conductivity and volume specific heat capacity both exhibit an increasing−decreasing trend from **SO350** to **SO520**. Therefore, the increase in the ratio of thermal conductivity is less than that of the volumetric specific heat capacity with respect to **SO350** to **SO400**, and the decrease in ratio of thermal conductivity is greater than that of volumetric specific heat capacity with respect to **SO400** to **SO520**.

3.4.4. Comparison of AR and OP processes

Composition and pore evolution are noted to exhibit different influences on the thermophysical properties of semi-cokes obtained via AR and OP. As shown in Fig. 15, the content of organic matter in semi-cokes obtained via AR processes gradually decreases with increasing pyrolysis temperatures, whereas the residual carbon content and pore volumes gradually increase [8]. Therefore, a high porosity and residual carbon content can only be obtained at extremely high temperatures, which indicates that the pore volume has a more obvious influence on the thermophysical properties of semi-cokes obtained from AR processes at high temperatures. The semi-cokes obtained from OP processes could possess a low content of organic residues and large pore volume at low temperatures [7,10], indicating that pore volume can significantly affect the thermophysical properties of semi-cokes at low temperatures in the OP process.

Generally, oil shale must be heated to more than 500 °C to obtain a higher oil yield in AR, whereas only ~ 350 °C is required in OP [6–9]. As shown in Figs. 12, 13, and 14, **SO350** exhibits a higher thermal conductivity, higher thermal diffusivity, and lower volumetric specific heat capacity than those of **SN520**. Therefore, OP offers more advantages in terms of heat transfer performance than those of the AR process.

4. Conclusion

Semi-cokes obtained via oxidizing pyrolysis (OP) exhibit different performances in terms of composition, pore evolution, and thermophysical properties compared to those obtained via anaerobic retorting (AR); the effects of composition and pore evolution on thermophysical properties of shale oil were analysed. The important conclusions are as follows: (1) Montmorillonite transforms into kaolinite and illite in OP, and into illite to form an illite/montmorillonite mixed layer in AR. (2) The specific surface area and pore volume of semi-cokes are extremely low at low temperatures in AR, whereas numerous mesopores and macropores can be formed in OP, leading to significant increases in the specific surface area and pore volume even at low temperatures. (3) Variations in chemical composition and pore evolution of semi-cokes obtained via AR and OP affected their thermophysical properties. The thermophysical properties of semi-cokes obtained via OP are expected to favour the in-situ exploitation of oil shale.

CRediT authorship contribution statement

Shaotao Xu: Writing - review & editing, Methodology. **Youhong Sun:** Supervision, Conceptualization. **Xiaoshu Lü:** Supervision, Validation. **Qinchuan Yang:** Resources. **Qiang Li:** Validation. **Zhendong Wang:** Validation. **Mingyi Guo:** Conceptualization, Methodology.

Declaration of Competing Interest

The authors declare that they have no known competing financial interests or personal relationships that could have appeared to influence

the work reported in this paper.

Acknowledgements

This work was supported by the China Postdoctoral Science Foundation (No. 2019 M651210), China Postdoctoral International Postdoctoral Exchange Fellowship Program (20190056), Youth Science Foundation of Jilin Province (20190103138JH), the Science and Technology Development Project of Jilin Province, China (Grant No. 20200201221JC), National Key R&D Program of China (No. 2019YFA0705502, 2019YFA0705501).

Appendix A. Supplementary data

Supplementary data to this article can be found online at https://doi.org/10.1016/j.fuel.2021.121565.

References

[1] Kamyk J, Kot-Niewiadomska A, Galos K. The criticality of crude oil for energy security: A case of Poland. Energy 2021;220:119707. https://doi.org/10.1016/j.energy.2020.119707.

[2] kafazi IE, Bannari R, Aboutafail MO. The impact of predicted demand on energy production. IOP Conference Series: Earth and Environmental Science 2018;154:012006. https://doi.org/10.1088/1755-1315/154/1/012006.

[3] Kuang W, Lu M, Yeboah I, Qian G, Duan X, Yang J, et al. A comprehensive kinetics study on non-isothermal pyrolysis of kerogen from Green River oil shale. Chem Eng J 2019;377:120275. https://doi.org/10.1016/j.cej.2018.10.212.

[4] Yang S, Yang D, Kang Z. Experimental investigation of the anisotropic evolution of tensile strength of oil shale under real-time high-temperature conditions. Nat Resour Res 2021;30(3):2513–28.

[5] He W, Sun Y, Shan X. Organic matter evolution in pyrolysis experiments of oil shale under high pressure: Guidance for in situ conversion of oil shale in the Songliao Basin. J Anal Appl Pyrol 2021;155:105091. https://doi.org/10.1016/j.jaap.2021.105091.

[6] Kang Z, Zhao Y, Yang D. Review of oil shale in-situ conversion technology. Appl Energy 2020;269:115121. https://doi.org/10.1016/j.apenergy.2020.115121.

[7] Guo H, Peng S, Lin J, Chang J, Lei S, Fan T, et al. Retorting oil shale by a self-heating route. Energy Fuels 2013;27(5):2445–51.

[8] Guo W, Yang Q, Sun Y, Xu S, Kang S, Lai C, et al. Characteristics of low temperature co-current oxidizing pyrolysis of Huadian oil shale. J Anal Appl Pyrol 2020;146:104759. https://doi.org/10.1016/j.jaap.2019.104759.

[9] Sun Y-H, Bai F-T, Lü X-S, Li Q, Liu Y-M, Guo M-Y, et al. A novel energy-efficient pyrolysis process: self-pyrolysis of oil shale triggered by topochemical heat in a horizontal fixed bed. Sci Rep 2015;5(1). https://doi.org/10.1038/srep08290.

[10] Guo H, Pei Y, Wang K, Cheng Q, Ding Y, Jin Ze, et al. Identifying the reaction mechanism of oil-shale self-heating retorting by thermal analysis techniques. Fuel 2015;160:255–64.

[11] Guo H, Yang Y, Wang K, Pei Y, Wu Q, Liu Y. Strengthening the applicability of self-heating retorting process to oil shale via co-retorting. Fuel 2015;143:1–8.

[12] Sun Y, Bai F, Liu B, Liu Y, Guo M, Guo W, et al. Characterization of the oil shale products derived via topochemical reaction method. Fuel 2014;115:338–46.

[13] Wang G, Yang D, Kang Z, Zhao J. Anisotropy in thermal recovery of oil shale-Part 1: Thermal conductivity, wave velocity and crack propagation. Energies 2018;11(1):77. https://doi.org/10.3390/en11010077.

[14] Sun Q, Chen SE, Gao Q, Zhang WQ, Geng JS, Zhang YL. Analyses of the factors influencing sandstone thermal conductivity. Acta Geodyn Geomater 2017;2(186):173–80.

[15] Ma Y, He Lu, Li S, Teng J. Heat transfer of oil shale in a small-scale fixed bed. J Therm Anal Calorim 2016;124(1):461–9.

[16] Jha MK, Verma AK, Maheshwar S, Chauhan A. Study of temperature effect on thermal conductivity of Jhiri shale from Upper Vindhyan, India. Bull Eng Geol Environ 2015;75(4):1–12.

[17] Askari R, Taheri S, Hejazi SH. Thermal conductivity of granular porous media: A pore scale modeling approach. AIP Adv 2015;5(9):097–106.

[18] Gunn DA, Jones LD, Raines MG, Entwisle DC, Hobbs PRN. Laboratory measurement and correction of thermal properties for application to the rock mass. Geotech Geol Eng 2005;23(6):773–91.

[19] Wen Hu, Lu J-H, Xiao Y, Deng J. Temperature dependence of thermal conductivity, diffusion and specific heat capacity for coal and rocks from coalfield. Thermochim Acta 2015;619:41–7.

[20] Krishnaiah S, Singh DN, Jadhav GN. A methodology for determining thermal properties of rocks. Int J Rock Mech Min Sci 2004;41(5):877–82.

[21] Ma Y, Li S. The mechanism and kinetics of oil shale pyrolysis in the presence of water. Carbon Resour Convers 2018;1(2):160–4.

[22] Guo H, Lin J, Yang Y, Liu Y. Effect of minerals on the self-heating retorting of oil shale: Self-heating effect and shale-oil production. Fuel 2014;118:186–93.

[23] Zhang JC, Li BX, Meng J, Li YZ, Wang XF, Liu XY, et al. Transformation of montmorillonite illitization based on hydrothermal experiments. Global geology 2018;37:316–26.

[24] Jin PP, Ou CH, Ma ZG, Li D, Ren YJ, Zhao YF. Evolution of montmorillonite and its related clay minerals and their effects on shale gas development. Geophys Prospect Petrol 2018;57:344–55.

[25] Tiwari P, Deo M. Detailed kinetic analysis of oil shale pyrolysis TGA data. AIChE J 2012;58(2):505–15.

[26] Lai D, Zhan J-H, Tian Y, Gao S, Xu G. Mechanism of kerogen pyrolysis in terms of chemical structure transformation. Fuel 2017;199:504–11.

[27] Bai F, Sun Y, Liu Y, Guo M. Evaluation of the porous structure of Huadian oil shale during pyrolysis using multiple approaches. Fuel 2017;187:1–8.

[28] Bai F, Guo W, Lü X, Liu Y, Guo M, Li Q, et al. Kinetic study on the pyrolysis behavior of Huadian oil shale via non-isothermal thermogravimetric data. Fuel 2015;146:111–8.

[29] Martins MF, Salvador S, Thovert J-F, Debenest G. Co-current combustion of oil shale-Part 1: Characterization of the solid and gaseous products. Fuel 2010;89(1):144–51.

[30] Sun Y, Bai F, Lü X, Jia C, Wang Q, Guo M, et al. Kinetic study of Huadian oil shale combustion using a multi-stage parallel reaction model. Energy 2015;82:705–13.

[31] Bai F, Sun Y, Liu Y, Li Q, Guo M. Thermal and kinetic characteristics of pyrolysis and combustion of three oil shales. Energy Convers Manage 2015;97:374–81.

[32] Liu Z, Yang D, Hu Y, Zhang J, Shao J, Song Su, et al. Influence of in situ pyrolysis on the evolution of pore structure of oil shale. Energies 2018;11(4):755. https://doi.org/10.3390/en11040755.

[33] YANG L, YANG D, ZHAO J, LIU Z, KANG Z. Changes of oil shale pore structure and permeability at different temperatures. Oil Shale 2016;33(2):101. https://doi.org/10.3176/oil.2016.2.01.

[34] Jiang XM, Han XX, Cui ZG. Mechanism and mathematical model of Huadian oil shale pyrolysis. J Therm Anal Calorim 2006;86(2):457–62.

[35] Bai F, Sun Y, Liu Y, Guo M, Zhao J. Characteristics and kinetics of Huadian oil shale pyrolysis via non-isothermal thermogravimetric and gray relational analysis. Combust Sci Technol 2020;192(3):471–85.

[36] Sun Y, Xu S, Yang Q, Lai C, Guo M. Oxidizing pyrolysis of Huadian oil shale and its product distribution. J China Univ Pet (Edition of Natural Science) 2021;45(2):149–56. https://doi.org/10.3969/j.issn.1673-5005.2021.02.018.